

Thermal convection in a cylindrical annulus heated laterally

S. Hoyas[★], H. Herrero[★] and A. M. Mancho[†]

[★] Departamento de Matemáticas, Facultad de Ciencias Químicas
Universidad de Castilla-La Mancha, 13071 Ciudad Real, Spain.

[†] Department of Mathematics, School of Mathematics
University of Bristol, University Walk,
Bristol BS8 1TW, United Kingdom.

E-mail: Sergio.Hoyas@uclm.es (S Hoyas), Henar.Herrero@uclm.es
(H Herrero) and A.M.Mancho@Bristol.ac.uk (A M Mancho)

October 30, 2018

Abstract

In this paper we study thermoconvective instabilities appearing in a fluid within a cylindrical annulus heated laterally. As soon as a horizontal temperature gradient is applied a convective state appears. As the temperature gradient reaches a critical value a stationary or oscillatory bifurcation may take place. The problem is modelled with a novel method which extends the one described in [10]. The Navier Stokes equations are solved in the primitive variable formulation, with appropriate boundary conditions for pressure. This is a low order formulation which in cylindrical coordinates introduces lower order singularities. The problem is discretized with a Chebyshev collocation method easily implemented and its convergence has been checked. The results obtained are not only in very good agreement with those obtained in experiments, but also provide a deeper insight into important physical parameters developing the instability, which has not been reported before.

1 Introduction

The problem of thermoconvective instabilities in fluid layers driven by a temperature gradient has become a classical subject in fluid mechanics [1, 2]. It is well known that two different effects are responsible for the onset of motion when the temperature difference becomes larger than a certain threshold: gravity and capillary forces. When both effects are taken into account the problem is called Bénard-Marangoni (BM) convection [3].

To solve numerically hydrodynamical problems in the primitive variable formulation raises two questions, one is the handling of first order derivatives for pressure and the other is finding its boundary conditions [4, 5, 6], which are not intuitive. In thermoconvective problems pressure usually is avoided, for instance in Refs. [7, 8] the method of potentials of velocity is used to eliminate it from the equations. This technique raises the order of the differential equations and additional boundary conditions may be required. This is particularly troublesome in cylindrical coordinates where high order derivatives cause awkward difficulties. In Ref. [9] the primitive variables formulation is used although the use of a particular spectral method allows the removal of pressure. In Ref. [10] the linear stability analysis of two convection problems are solved in the primitive variables formulation and taking appropriate boundary conditions for pressure. In this article very good accuracy is obtained both for cartesian and cylindrical coordinates. This method has been successfully applied to describe experimental results in cylindrical containers [11]. In this paper we extend this method to study a BM problem in a cylinder heated laterally.

The physical set up (Fig. 1) consists of a fluid filling up a container bounded by two concentric cylinders. The upper surface is open to the air and the fluid is heated laterally through the lateral walls which are conducting. This set up corresponds to the experiment reported in Ref. [12], and also it is comparable to similar experiments in rectangular containers [13, 14]. In [15] a similar problem is treated theoretically, however in this work rotation is considered and the gravity field is along the radial coordinate. In the problem we treat, as soon as a slight difference of temperature is imposed between the lateral walls, a stationary solution appears which is called basic state. When the temperature of the walls is modified the basic state can become unstable and bifurcate to different patterns, both stationary and oscillatory. When the bifurcation is stationary, the emerging pattern consists of a 3D structure of rolls whose axes are parallel to the radial coordinate (radial rolls) and in the oscillatory case, the axes are tilted with respect the radial axis. These results coincide with those obtained experimentally [12, 13, 14].

The basic state is calculated solving a set of nonlinear equations whereby the first contribution is obtained by a linear approach. To improve the solution we expand the corrections of the unknown fields in Chebyshev polynomials, and we

pose the equations at the Gauss-Lobatto collocation points [16]. The bifurcation thresholds are obtained through a generalized eigenvalue problem with the same Chebyshev collocation method. The convergence of the method is studied by comparing different expansions.

The organization of the article is as follows. In Sec. 2 the formulation of the problem with the equations and boundary conditions is explained. In the third section the basic state is calculated and the results obtained are discussed for different physical conditions. In the fourth section the linear stability of the basic solution is performed and instabilities are studied for different parameters. In the fifth section conclusions are detailed.

2 Formulation of the problem

The physical set up considered is shown in Fig. 1. A horizontal fluid layer of depth d (z coordinate) is in a container bounded by two concentric cylinders of radii a and $a+\delta$ (r coordinate). The bottom plate is rigid and the top is open to the atmosphere. The inner cylinder has a temperature T_{\max} whereas the outer one is at T_{\min} and the environment is at T_0 . We define $\Delta T = T_{\max} - T_0$ and $\Delta T_h = T_{\max} - T_{\min}$, which are the main two parameters controlling instabilities in this problem. The system evolves according to the momentum and mass balance equations and to the energy conservation principle. In the equations governing the system u_r , u_ϕ and u_z are the components of the velocity field u of the fluid, T the temperature, p the pressure, \mathbf{r} the radio vector and t the time are denoted. The magnitudes are expressed in dimensionless form after rescaling in the following form: $\mathbf{r}' = \mathbf{r}/d$, $t' = \kappa t/d^2$, $u' = du/\kappa$, $p' = d^2 p/(\rho_0 \kappa \nu)$, $\Theta = (T - T_0)/\Delta T$. Here κ is the thermal diffusivity, ν the kinematic viscosity of the liquid and ρ_0 is the mean density at the environment temperature T_0 .

The governing dimensionless equations (the primes in the corresponding fields have been dropped) are the continuity equation,

$$\nabla \cdot u = 0. \tag{1}$$

The energy balance equation,

$$\partial_t \Theta + u \cdot \nabla \Theta = \nabla^2 \Theta, \tag{2}$$

The Navier-Stokes equations,

$$\partial_t u + (u \cdot \nabla) u = Pr \left(-\nabla p + \nabla^2 u + \frac{R\rho}{\alpha\rho_0\Delta T} e_z \right), \tag{3}$$

where the operators and fields are expressed in cylindrical coordinates [5] and e_z is the unit vector in the z direction. Here the Oberbeck-Boussinesq approximation has been used. It consist of considering only in the buoyant term, the following density dependence on temperature $\rho = \rho_0 [1 - \alpha (T - T_0)]$, where α is the thermal expansion coefficient. The following dimensionless numbers have been introduced:

$$Pr = \frac{\nu}{\kappa}, \quad R = \frac{g\alpha\Delta T d^3}{\kappa\nu}, \quad (4)$$

where g is the gravity constant. Pr is the Prandtl number which is assumed to have a large value and R the Rayleigh number, representative of the buoyancy effect.

2.1 Boundary conditions

We discuss now the boundary conditions (bc). The top surface is flat, which implies the following condition on the velocity,

$$u_z = 0, \quad \text{on } z = 1. \quad (5)$$

The variation of the surface tension with temperature is considered: $\sigma(T) = \sigma_0 - \gamma(T - T_0)$, where σ_0 is the surface tension at temperature T_0 , γ is the constant rate of change of surface tension with temperature (γ is positive for most current liquids). This effect supplies the Marangoni conditions for the velocity fields which in dimensionless form are,

$$\partial_z u_r + M \partial_r \Theta = 0, \quad \partial_z u_\phi + \frac{M}{r} \partial_\phi \Theta = 0, \quad \text{on } z = 1. \quad (6)$$

Here $M = \gamma\Delta T d / (\kappa\nu\rho_0)$ is the Marangoni number. In our particular problem the Rayleigh and the Marangoni numbers are related in the same way as in the experiments in Ref. [12] $M = 9.2 \cdot 10^{-8} R/d^2$, so buoyancy effects are dominant. The remaining boundary conditions correspond to rigid walls and are expressed as follows,

$$u_r = u_\phi = u_z = 0, \quad \text{on } z = 0, \quad (7)$$

$$u_r = u_\phi = u_z = 0, \quad \text{on } r = a^*, \quad r = a^* + \delta^*, \quad (8)$$

where $a^* = a/d$ and $\delta^* = \delta/d$.

For temperature we consider the dimensionless form of Newton's law for heat exchange at the surface,

$$\partial_z \Theta = -B\Theta, \quad \text{on } z = 1, \quad (9)$$

where B is the Biot number. At the bottom a linear profile is imposed,

$$\Theta = \left(-\frac{r}{\delta^*} + \frac{a}{\delta} \right) \frac{\Delta T_h}{\Delta T} + 1, \quad \text{on } z = 0, \quad (10)$$

while in the lateral walls conducting boundary conditions are considered

$$\Theta = 1, \text{ on } r = a^*, \quad (11)$$

$$\Theta = \left(-1 + \frac{a}{\delta}\right) \frac{\Delta T_h}{\Delta T} + 1, \text{ on } r = a^* + \delta^*. \quad (12)$$

From this boundary conditions it is clear how not only ΔT defining the Rayleigh number is involved in the problem, but also ΔT_h . Due to the fact that pressure is kept in the equations, additional boundary conditions are needed. They are obtained by the continuity equation at $z = 1$ and the normal component of the momentum equations on $r = a^*$, $r = a^* + \delta^*$ and $z = 0$, [10].

$$\nabla \cdot u = 0, \text{ on } z = 1, \quad (13)$$

$$\begin{aligned} Pr^{-1} \left(\frac{\partial u_r}{\partial t} + u_r \frac{\partial u_r}{\partial r} + \frac{u_\phi}{r} \frac{\partial u_r}{\partial \phi} + u_z \frac{\partial u_r}{\partial z} - \frac{u_\phi^2}{r} \right) = \\ = -\frac{\partial p}{\partial r} + \Delta u_r - \frac{u_r}{r^2} - \frac{2}{r^2} \frac{\partial u_\phi}{\partial \phi}, \text{ on } r = a^*, r = a^* + \delta^*, \end{aligned} \quad (14)$$

$$\begin{aligned} Pr^{-1} \left(\frac{\partial u_z}{\partial t} + u_r \frac{\partial u_z}{\partial r} + \frac{u_\phi}{r} \frac{\partial u_z}{\partial \phi} + u_z \frac{\partial u_z}{\partial z} \right) = \\ = -\frac{\partial p}{\partial z} + \Delta u_z - b + RT, \text{ on } z = 0, \end{aligned} \quad (15)$$

where $b = d^3 g / (\kappa \nu)$, and $\Delta = r^{-1} \partial / \partial r (r \partial / \partial r) + r^{-2} \partial^2 / \partial \phi^2 + \partial^2 / \partial z^2$.

3 Basic state

As soon as the lateral walls are at different temperatures and a horizontal temperature gradient is set at the bottom, a stationary convective motion appears in the fluid. In contrast to the classical Bénard-Marangoni problem with uniform heating, here the basic state is not conductive, but convective. In order to calculate it, for computational convenience, the following change has been performed: $r' = 2r/\delta^* - 2a^*/\delta^* - 1$ and $z' = 2z - 1$, which transforms the domain $\Omega_1 = [a^*, a^* + \delta^*] \times [0, 2\pi] \times [0, 1]$ into $\Omega = [-1, 1] \times [0, 2\pi] \times [-1, 1]$. After these changes, and since the basic state has radial symmetry (there is no dependence on ϕ) the steady state equations in the infinite Prandtl number approach become (the primes have been dropped),

$$A \partial_r p + G^2 u_r = \Delta^* u_r, \quad (16)$$

$$2 \partial_z p + b - R \Theta = \Delta^* u_z, \quad (17)$$

$$G u_r + A \partial_r u_r + 2 \partial_z u_z = 0, \quad (18)$$

$$u_r A \partial_r \Theta + 2 u_z \partial_z \Theta = \Delta^* \Theta, \quad (19)$$

where $\Delta^* = A^2 \partial_r^2 + GA \partial_r + 4 \partial_z^2$, $b = d^3 g / \kappa \nu$, $A = 2d / \delta$ and $G(r) = 2d / (2a + \delta + r\delta)$.

The boundary conditions are now as follows,

$$u_z = 2\partial_z u_r + MA \partial_r T = 2\partial_z \Theta + B\Theta = 0, \quad \text{on } z = 1, \quad (20)$$

$$Gu_r + A \partial_r u_r + 2\partial_z u_z = 0, \quad \text{on } z = 1, \quad (21)$$

$$u_r = u_z = 0, \Theta = (1 - r)/2, \quad \text{on } z = -1, \quad (22)$$

$$2\partial_z p + b - R\Theta = \Delta^* u_z, \quad \text{on } z = -1, \quad (23)$$

$$u_r = u_z = 0, \Theta = 0, \quad \text{on } r = 1, \quad (24)$$

$$A \partial_r p + G^2 u_r = \Delta^* u_r, \quad \text{on } r = 1, \quad (25)$$

$$u_r = u_z = 0, \Theta = 1, \quad \text{on } r = -1, \quad (26)$$

$$A \partial_r p + G^2 u_r = \Delta^* u_r, \quad \text{on } r = -1. \quad (27)$$

3.1 Numerical method

We have solved numerically Eqs. (16)-(19) together with the boundary conditions (20)-(27) by a Chebyshev collocation method. This approximation is given by four perturbation fields $u_r(r, z)$, $u_z(r, z)$, $p(r, z)$ and $\Theta(r, z)$ which are expanded in a truncated series of orthonormal Chebyshev polynomials:

$$u_r(r, z) = \sum_{n=0}^N \sum_{m=0}^M a_{nm} T_n(r) T_m(z), \quad (28)$$

$$u_z(r, z) = \sum_{n=0}^N \sum_{m=0}^M b_{nm} T_n(r) T_m(z), \quad (29)$$

$$p(r, z) = \sum_{n=0}^N \sum_{m=0}^M c_{nm} T_n(r) T_m(z), \quad (30)$$

$$\Theta(r, z) = \sum_{n=0}^N \sum_{m=0}^M d_{nm} T_n(r) T_m(z). \quad (31)$$

Expressions (28)-(31) are replaced into the equations (16)-(19) and boundary conditions (20)-(26). The $N+1$ Gauss-Lobato points ($r_j = \cos(\pi(1 - j/N))$, $j = 0, \dots, N$) in the r axis and the $M+1$ Gauss-Lobato points ($z_j = \cos(\pi(1 - j/M))$, $j = 0, \dots, M$) in the z axis are calculated. The previous equations are evaluated at these points according to the rules explained in Ref. [17], in this way $4(N+1)(M+1)$ equations are obtained with $4(N+1)(M+1)$ unknowns. The system has not maximum rank because pressure is only determined up to a constant value. Since this value is not affecting to the other physical magnitudes, we replace the evaluation of the normal component of the momentum equations at ($r_{j=N} = 1$, $z_{j=4} = \cos(\pi(1 - 4/M))$) by a value for the pressure at this point, for instance $p = 0$. To solve the resulting nonlinear equations, a Newton-like iterative method is used. In a first step the nonlinearity

is discounted and a solution is found by solving the linear system. It is corrected by small perturbation fields: $\bar{u}_r(r, z)$, $\bar{u}_z(r, z)$, $\bar{p}(r, z)$ and $\bar{\Theta}(r, z)$,

$$u_r^{i+1}(r, z) = u_r^i(r, z) + \bar{u}_r(r, z), \quad (32)$$

$$u_z^{i+1}(r, z) = u_z^i(r, z) + \bar{u}_z(r, z), \quad (33)$$

$$p^{i+1}(r, z) = p^i(r, z) + \bar{p}(r, z), \quad (34)$$

$$\Theta^{i+1}(r, z) = \Theta^i(r, z) + \bar{\Theta}(r, z), \quad (35)$$

in such way that solutions at $i + 1$ step are obtained after solving Eqs. (16)-(26) linearized around the approach at step i . The considered criterion of convergence is that the difference between two consecutive approximations in l^2 norm should be smaller than 10^{-9} .

3.2 Results on the basic state

Previous theoretical works [18, 19, 20] dealing with this problem have approached the basic state solution as a parallel flow, where only the horizontal component of the velocity field exists. This approach requires the imposition of a constant temperature gradient over all the fluid layer and at the top boundary. In those descriptions this gradient becomes the main control parameter. In our model lateral effects are considered, so parallel flow is no longer valid and no restrictions are needed in the temperature boundary conditions which, as explained in the previous section, is the usual Newton law. This boundary condition is the origin of two control parameters related to temperature, i. e., ΔT_h and ΔT . This possibility, which had been already addressed in [21], is explored in detail in the next section.

We have found two types of basic states. The first one, displayed in Fig. 2 shows the isotherms obtained at $B = 1.25$, $\delta^* = 10$ and $\Delta_h T = \Delta T = 6.4^\circ \text{C}$. The bottom profile is linear, as expected from the boundary condition, however at the top it approaches the constant ambient temperature, since the Biot number is large. This field is similar to that of the layer heated from below, i.e. roughly speaking hotter at the bottom. This feature is shared with the *linear flow* described in [20]. Fig. 3 shows the velocity fields for the same conditions. They are formed by two co-rotative rolls perpendicular to the gradient. This result is similar to that obtained in experiments reported in Refs. [12, 13, 14], where co-rotative rolls perpendicular to the gradient are found as well. These results coincide with those obtained in Ref. [21] for a rectangular geometry.

The second kind of basic state is represented in Fig. 4 for $B = 0.8$, $\delta^* = 2.5$, $\Delta_h T = 0.3^\circ \text{C}$, $\Delta T = 1.84^\circ \text{C}$. The most striking feature is that along the vertical axis there are changes in the sign of the temperature gradient. It seems that the Biot number is not dissipating heat effectively at the top and then heat is advected

by the velocity field. This temperature profile coincides with that of the *return flow* defined in Ref. [20], where the role of the transport of heat by the velocity field as the origin of the instability is discussed. As we will demonstrate in the next section this flow becomes unstable through an oscillatory bifurcation, as it is also reported in [20]. Crucial to the appearance of the two different flows described in this section, is not only the Biot number that dissipates heat at the top, but also the role of parameters ΔT and ΔT_h which introduces heat into the system.

Fig. 5 shows a transition between the two states we have just described. It is obtained at $B = 0.3$, $\delta^* = 10$, $\Delta_h T = 10^\circ \text{C}$, $\Delta T = 20.41^\circ \text{C}$. At this stage the flow already becomes unstable through an oscillatory bifurcation.

4 Linear stability of the basic state

The stability of the basic state is studied by perturbing it with a vector field depending on the r, ϕ and z coordinates, in a fully 3D analysis:

$$u_r(r, \phi, z) = u_r^b(r, z) + \bar{u}_r(r, z) e^{im\phi + \lambda t}, \quad (36)$$

$$u_\phi(r, \phi, z) = u_\phi^b(r, z) + \bar{u}_\phi(r, z) e^{im\phi + \lambda t}, \quad (37)$$

$$u_z(r, \phi, z) = u_z^b(r, z) + \bar{u}_z(r, z) e^{im\phi + \lambda t}, \quad (38)$$

$$\Theta(r, \phi, z) = \Theta^b(r, z) + \bar{\Theta}(r, z) e^{im\phi + \lambda t}, \quad (39)$$

$$p(r, \phi, z) = p^b(r, z) + \bar{p}(r, z) e^{im\phi + \lambda t}. \quad (40)$$

Here the superscript b indicates the corresponding quantity in the basic state and the bar refers to the perturbation. We have considered Fourier modes expansions in the angular direction, because along it the boundary conditions are periodic. We replace the expressions (36)-(40) into the basic equations and after linearizing the resulting system, we obtain the following eigenvalue problem (the bars have been dropped):

$$\Delta_m u_r - A \partial_r p - G^2 u_r - 2G^2 i m u_\phi = 0, \quad (41)$$

$$\Delta_m u_\phi - G i m p + 2G^2 i m u_r - G^2 u_\phi = 0, \quad (42)$$

$$\Delta_m u_z - 2 \partial_z p + R \Theta = 0, \quad (43)$$

$$G u_r + A \partial_r u_r + G i m u_\phi + 2 \partial_z u_z = 0, \quad (44)$$

$$\Delta_m \Theta - u_r A \partial_r \Theta^b - u_r^b A \partial \Theta - 2 u_z^b \partial_z \Theta - 2 u_z \partial_z \Theta^b = \lambda \Theta, \quad (45)$$

where $\Delta_m = A^2 \partial_r^2 + G A \partial_r - m^2 G^2 + 4 \partial_z^2$. The following boundary conditions for the perturbations are obtained,

$$u_z = 2 \partial_z u_r + M A \partial_r \Theta = 2 \partial_z u_\phi + G M i m \Theta = 2 \partial_z \Theta + B \Theta = 0, \quad \text{on } z = 1, \quad (46)$$

$$u_r = u_\phi = u_z = \Theta = 0, \text{ on } z = -1, \quad (47)$$

$$u_r = u_\phi = u_z = 0, \Theta = 0, \text{ on } r = 1, \quad (48)$$

$$u_r = u_\phi = u_z =, \Theta = 0, \text{ on } r = -1, \quad (49)$$

together with

$$\Delta_m u_r - A \partial_r p - 2G^2 i m u_\phi = 0, \text{ on } r = \pm 1, \quad (50)$$

$$\Delta_m u_z - 2 \partial_z p + R \Theta = 0, \text{ on } z = -1, \quad (51)$$

$$G u_r + A \partial_r u_r + G i m u_\phi + 2 \partial_z u_z = 0, \text{ on } z = 1. \quad (52)$$

4.1 Numerical method

The eigenvalue problem is discretized with the Chebyshev collocation method used for the basic state. Now there is a new field, the angular velocity, which is expanded as follows,

$$u_\phi(r, z) = \sum_{n=0}^N \sum_{m=0}^M e_{nm} T_n(r) T_m(z). \quad (53)$$

In order to calculate the eigenfunctions and thresholds of the generalized eigenvalue problem the equations are posed at the collocation points according to the rules explained in [17], so that a total of $5(N+1)(M+1)$ algebraic equations are obtained with the same number of unknowns. If the coefficients of the unknowns which form the matrices A and B satisfy $\det(A - \lambda B) = 0$, a nontrivial solution of the linear homogeneous system exists. This condition generates a dispersion relation $\lambda \equiv \lambda(m, R, M, B, u^b, \Theta^b, p^b)$, equivalent to calculate directly the eigenvalues from the system $AX = \lambda BX$, where X is the vector which contains the unknowns. If $\text{Re}(\lambda) < 0$ the basic state is stable while if $\text{Re}(\lambda) > 0$ the basic state becomes unstable. In the Appendix a study of the convergence of the thresholds calculated with this method is shown.

4.2 Results on the stability analysis

The basic solutions obtained in section 3, become unstable when the control parameter, ΔT in this work, is increased. When ΔT is changed, ΔT_h which is not the control parameter in our choice, is fixed to a non zero value. In the explored parameter range two types of bifurcations take place: stationary and oscillatory. Figure 6 depicts the m dependence of $\text{Re}(\lambda)$ for $B = 1.25$, $\delta^* = 10$ and $\Delta T_h = \Delta T$ at the threshold ($\Delta T_c = 6.4^\circ \text{C}$) and below it ($\Delta T < 6.4^\circ \text{C}$). The bifurcation is stationary since the imaginary part of the eigenvalue λ is zero at the critical value $m_c = 20$. Figure 7 is similar to Figure 6 but at $B = 0.5$, $\delta^* = 10$ and $\Delta T_h = 5^\circ \text{C}$

and $\Delta T_c = 8.63^\circ\text{C}$. Now the bifurcation is oscillatory since the imaginary part of the eigenvalue is non zero at the critical value $m_c = 18$. In order to understand how physical conditions affect the instability, Fig. 8 summarizes the influence of heat related parameters in the bifurcation. There, it is shown the critical value of ΔT_c , as a function of the Biot number B , for several values of ΔT_h . In this figure stationary and oscillatory bifurcations are observed and it shows that having one or other transition depends on an equilibrium between these parameters. Travelling waves are favoured by systems storing a lot of heat, i.e., low values of the Biot number, and high values of $\Delta_h T$, which facilitates the transport of heat by the velocity field [20]. We notice here the novelty of these results, where transitions between stationary rolls and oscillatory waves are due to changes in heat related parameters. This has not been reported in any experimental or theoretical work before, where transitions have been found due to variations in Prandtl number [20] or in aspect ratio [13, 14].

In Fig. 8 it is also clear that thresholds decrease as B increases while the dependence of thresholds on ΔT_h is not monotonous, it presents a minimum for $\Delta T_h = 2^\circ\text{C}$ as figure 9 a) displays. In Fig. 9 b) it is shown how the critical wavenumber increases with ΔT_h , on the other hand it remains almost constant with B .

The geometry and size of the box is also affecting the instability as it is noticed mainly in low aspect ratio systems. Although a detailed study of patterns in small containers is beyond the scope of this work, table I gives an insight into it. It shows the critical value of ΔT_c and the corresponding critical wavenumber m_c for some δ^* . The wavenumber does not change monotonously with the aspect ratio, as also happens in small containers with uniform heating from below [9, 10, 11] as well.

The critical wavenumber for the stationary bifurcation shows that a 3D structure appears which consists of radial rolls whose axes are parallel to the radial coordinate as Fig. 10 shows for $B = 1.25$ and $\delta^* = 10$ and $\Delta T_c = 6.4^\circ\text{C}$. The growing perturbation along the transverse plane is plotted in Fig. 11, where a structure appears near the hot side as in the experiment reported in [23]. This is so because, in this case, the instability has the same origin as a static fluid heated from below, so since the vertical temperature gradient is greater at this boundary, perturbation grows there first. On the other hand since the hot cylinder counteracts the vertical temperature gradient it inhibits the instability threshold. These results are in good agreement with those obtained in Ref. [21] in similar conditions but in a cartesian geometry. In that article at a threshold $\Delta T_c = 6.8^\circ\text{C}$, the critical wavenumber is $k_c = 2.4$, which would correspond to 12 – 36 periods respectively in the inner and outer radii of an annulus as ours. This matches rather well with our critical threshold and wavenumber which is $m_c = 20$, suggesting that, at least for this aspect ratio, geometry does not strongly affect the results. These results and discussions

of the stationary bifurcation are in good agreement with those reported in Refs. [13, 18, 19, 20, 22].

We also obtain oscillatory bifurcations. For instance, there is one at $\delta^* = 10$ ($d = 2$ mm), $\Delta T_h = 5^\circ\text{C}$, $B = 0.5$ and $\Delta T_c = 8.63^\circ\text{C}$, which corresponds to travelling waves or hydrothermal waves described in Refs. [13, 12, 14]. Fig. 12 depicts the eigenfunction along the transverse plane, where the tilted axis of the waves can be seen. This result is comparable to that reported in Ref. [14] where for a cartesian container with $L_x = 20$ mm, $d \sim 2$ mm, hydrothermal waves of wavenumber $k_c \sim 1$, emerge above a threshold. This would correspond to a pattern with 6 – 19 periods in the inner and outer radii of our annulus respectively, which is not far from our critical wavenumber $m_c = 18$. The angle of inclination of the waves in Fig. 10 is $\phi \sim 3\pi/4$ also close to that of 2.60 – 1.75 rad of Ref. [14].

5 Conclusions

We have studied a BM lateral heating problem in a cylindrical annulus. The problem has been solved with a Chebyshev collocation method by keeping the original Navier-Stokes equations, where appropriate boundary conditions are required for pressure [10]. The scheme developed in Ref. [10] for stability problems has been extended to calculate a non trivial basic state. The procedure is confirmed to be reliable, effective and easy to implement.

We have obtained two kinds of basic solutions. One type is formed by corotative rolls such as those reported in experiments [12, 13, 14], and in similar theoretical studies [21]. The second kind of solution has similar features to those of the *return flow* described in [20].

The linear stability analysis of these solutions shows stationary bifurcations to radial rolls and oscillatory bifurcations to hydrothermal waves, whose appearance has been proved to depend on their heat related parameters (B , ΔT_h and ΔT). This fact has not been addressed before, perhaps because experimentally these parameters are hard to manipulate. Properties of the growing patterns coincide with those reported in previous works. Stationary solutions appear in basic flows with temperature profiles close to the static fluid heated from below [21, 20]. Their wavenumbers are in the range of experimental [12, 13, 14] and theoretical studies [21]. Also the structure in the $z - r$ plane agrees with previous results [21, 23]. Oscillatory solutions emerge from a basic state of the type of *return flow* as predicted in [20]. Their structure is comparable to that obtained in experiments [14].

Acknowledgments

We gratefully thank Christine Cantell, Maureen Mullins and Angel Garcimartín for useful comments and suggestions. This work was partially supported by

a Research Grant MCYT (Spanish Government) BFM2000-0521 and by the University of Castilla-La Mancha.

References

- [1] Bénard H 1900 *Rev. Gén. Sci. Pures Appl.* **11** 1261
- [2] Pearson J R A 1958 *J. Fluid Mech.* **4** 489
- [3] Nield D A 1964 *J. Fluid Mech.* **19** 341.
- [4] Gresho P M and Sani R L 1987 *Int. J. Num. Meth. Fluids* **7** 1111
- [5] Pozrikidis C 1997 *Introduction to theoretical and computational fluid dynamics* (Oxford: Oxford University Press)
- [6] Orszag S A, Israeli M and Deville O 1986 *J. Scient. Comp.* **1**(1) 75
- [7] Mercader I, Net M and Falques A 1991 *Comp. Methods Appl. Mech. and Engrg.* **91** 1245
- [8] Marqués F, Net M, Massaquer J M and Mercader I 1993 *Comp. Methods Appl. Mech. and Engrg.* **110** 157
- [9] Dauby P C, Lebon G and Bouhy E 1997 *Phys. Rev E* **56** 520
- [10] Herrero H and Mancho A M To appear in *Int. J. Numer. Methods Fluids*
<http://arXiv.org/abs/math.AP/0109200>
- [11] Ramón M L, Maza D M, Mancini H, Mancho A M and Herrero H 2001 *Int. J. of Bifurcation and Chaos* **11** (11) 2779
- [12] Ezersky A B, Garcimartín A, Burguete J, Mancini H L and C. Pérez-García C 1993 *Phys. Rev. E* **47** 1126
- [13] Daviaud F and Vince J M 1993 *Phys. Rev. E* **48** 4432
- [14] Burguete J, Mukolobwiesz N, Daviaud F, Garnier N and Chiffaudel A 2001 *Phys. Fluids* **13** 2773
- [15] Alonso M A 1999 *Ph. D. Thesis* (Barcelona: Universitat Politècnica de Catalunya)

- [16] Canuto C, Hussaini M Y, Quarteroni A and Zang T A 1988 *Spectral Methods in Fluid Dynamics* (Berlin: Springer)
- [17] Hoyas S, Herrero H and Mancho A M 2001 Actas del XVII CEDYA/VII CMA
- [18] Mercier J F and Normand C 1996 *Phys. Fluids* **8** 1433
- [19] Parmentier P, Regnier V and Lebon G 1993 *Int. J. Heat Mass Transfer* **36** 2417
- [20] Smith M K and Davis S H 1983 *J. Fluid Mech.* **132** 119
- [21] Mancho A M and Herrero H 2000 *Phys. Fluids* **12** 1044
- [22] Gershuni G Z, Laure P, Myznikov V M, Roux B and Zhukhovitsky E M 1992 *Microgravity Q* **2** 141
- [23] De Saedeleer C, Garcimartin A, Chavepeyer G, Platten J K and Lebon G 1996 *Phys. Fluids* **8**(3) 670
- [24] Mancho A M, Herrero H and Burguete J 1997 *Phys. Rev. E* **56** 2916
- [25] Hoyas S, Herrero H and Mancho A M, in preparation

Appendix

Convergence of the global numerical method

To carry out a test on the convergence of the global numerical method (calculation of the basic state and subsequent linear stability analysis) we compare the differences in the thresholds of the differences of temperature (ΔT) to different orders of expansions for some values of the parameters involved in the problem: $\delta^* \in [8.26, 10.52]$. In table II the thresholds for these states varying the aspect ratio are shown for four consecutive expansions varying the number of polynomials taken in the r (N) and z (M) coordinates. From the table it is seen that convergence is reached within a relative precision for ΔT_c of 10^{-2} . If M is increased the difference between successive expansions is order 10^{-1} while increasing N it is order 10^{-2} . Further increments of the order of the expansions give thresholds values oscillating around the quoted ones, so within that error, thresholds are convergent. The range of parameters has been selected in order to reach this convergence criterium.

Table captions

Table I

Critical ΔT and critical m_c vs the aspect ratio δ^* . The value of the horizontal temperature difference is $\Delta T_h = 0.4$ and $B = 1$.

Table II

Critical temperature differences ($^{\circ}\text{C}$) for different values of the aspect ratio at consecutive orders in the expansion in Chebyshev polynomials ($B = 1.25$).

Figure captions

Figure 1

Problem set up ($a = 0.01$ m, $\delta = 0.02$ m).

Figure 2

Isotherms of the basic state corresponding to values of the parameters $R = 2228$, $M = 51$, $\delta^* = 10$, $B = 1.25$ ($\Delta T = 6.4^{\circ}\text{C}$, $\Delta T_h = 6.4^{\circ}\text{C}$, $d = 2$ mm).

Figure 3

Velocity field at same conditions of Fig. 2.

Figure 4

Isotherms and velocity field of the basic state corresponding to values of the parameters $R = 40995$, $M = 59$, $\delta^* = 2.5$, $B = 0.8$ ($\Delta T = 1.84^{\circ}\text{C}$, $\Delta T_h = 0.3^{\circ}\text{C}$, $d = 8$ mm).

Figure 5

Isotherms and velocity field of the basic state corresponding to values of the parameters $R = 7105$, $M = 163$, $\delta^* = 10$, $B = 0.3$ ($\Delta T = 20.41^{\circ}\text{C}$, $\Delta T_h = 10^{\circ}\text{C}$, $d = 2$ mm).

Figure 6

Maximum real part of the growth rate λ as a function of m for basic state at $M = 51$, $\delta^* = 10$, $B = 1.25$. The top line stands for the threshold condition $R_c = 2228$ (or $\Delta T_c = 6.4^{\circ}\text{C}$), and its maximum determines the critical m_c . The bottom line is for $R < R_c$. Solid lines correspond to branches with real eigenvalues while the dotted ones stand for complex eigenvalues.

Figure 7

Maximum real part of the growth rate λ as a function of m for a basic state at $M = 69$, $\delta^* = 10$, $B = 0.5$, at the threshold condition $R_c = 3004$ (or $\Delta T_c = 8.63^\circ\text{C}$). The maximum determines the critical m_c . The solid line correspond to a branch with real eigenvalues while the dotted one is for complex eigenvalues.

Figure 8

Critical ΔT vs the Biot number B for different values of ΔT_h ($\delta^* = 10$).

Figure 9

Critical ΔT and m_c vs ΔT_h for $\delta^* = 10$ and $B = 0.7$.

Figure 10

Isotherms of the growing perturbation in the $x - y$ plane at a stationary bifurcation point ($\Delta T = \Delta T_h = 6.4^\circ\text{C}$, $\delta^* = 10$, $B = 1.25$).

Figure 11

a) Isotherms of the growing perturbation in the $r - z$ plane at a stationary bifurcation point ($\Delta T = \Delta T_h = 6.4^\circ\text{C}$, $\delta^* = 10$, $B = 1.25$). b) Velocity field of the growing perturbation in the $r - z$ plane at same conditions.

Figure 12

a) Isotherms of the eigenfunction in the $x - y$ plane at an oscillatory bifurcation point ($\Delta T_h = 5^\circ\text{C}$, $\Delta T = 8.63^\circ\text{C}$, $\delta^* = 10$, $B = 0.5$).

Figure 13

a) Isotherms of the eigenfunction in the $r - z$ plane at the oscillatory bifurcation point considered in Fig. 12. b) Velocity field of the eigenfunction in the $r - z$ plane at same conditions.

Table I

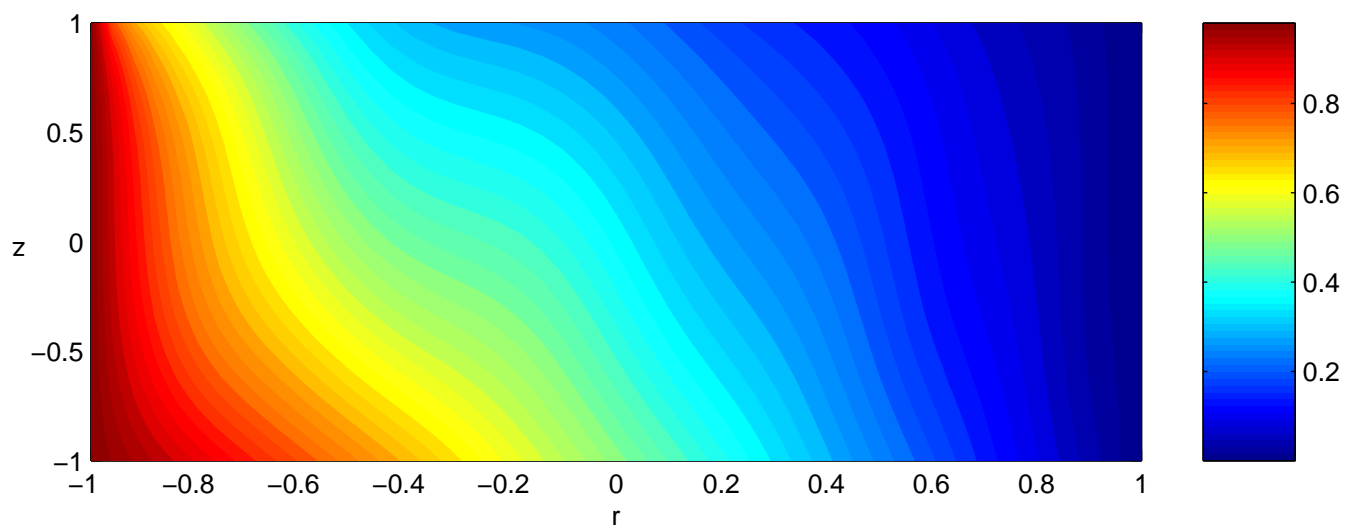
δ^*	ΔT_c	m_c
2.5	3.91	11
10/3	2.63	1
5	3.28	2
10	4.03	10

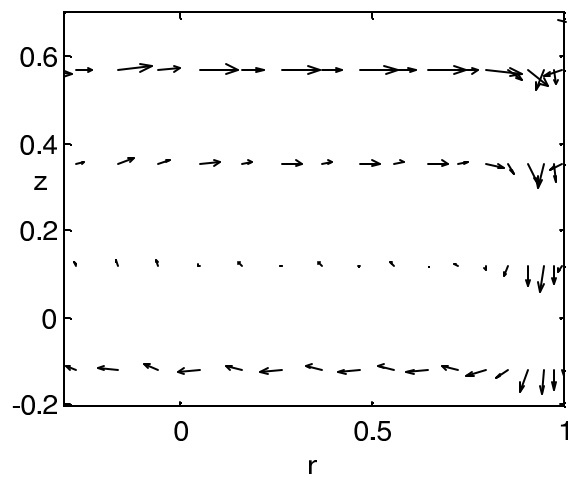
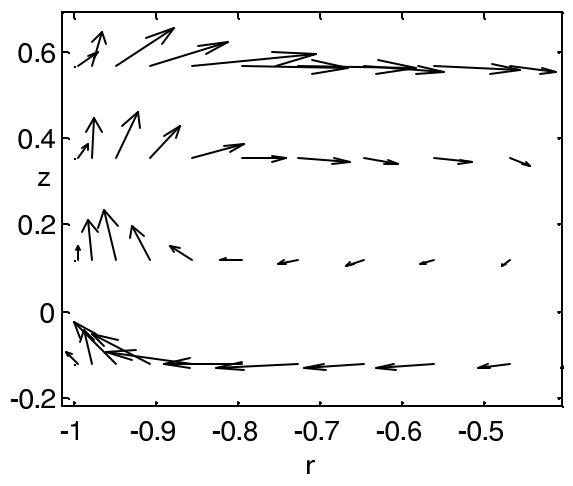
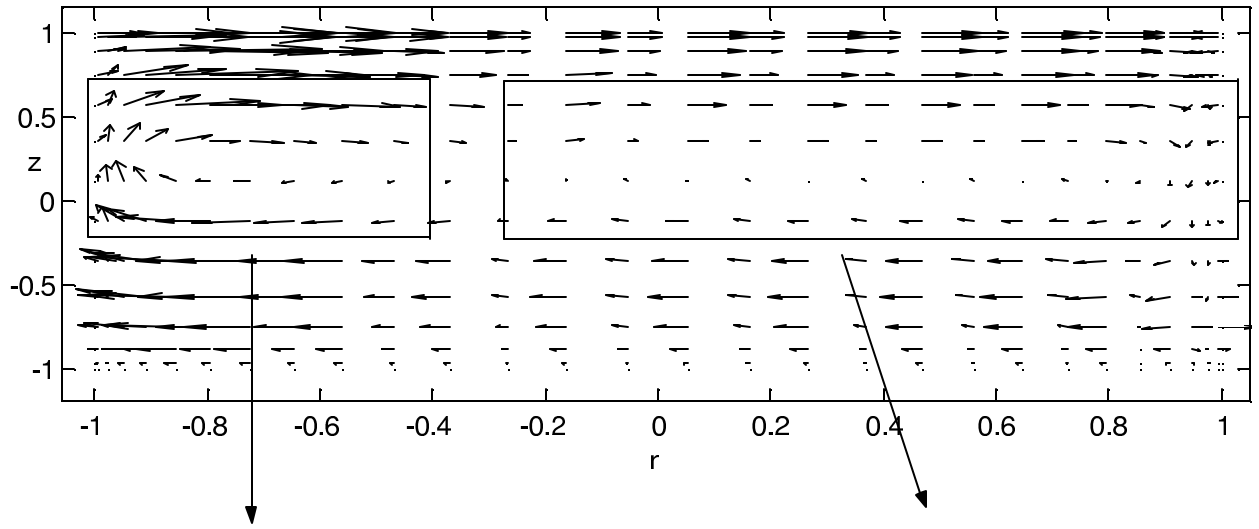
Table II

δ^*	13×9	13×13	25×13	29×13
10.52	6.8711	6.8519	6.9551	6.9229
10.25	6.5131	6.5224	6.6792	6.6665
10.00	6.2223	6.2298	6.3717	6.3938
9.52	5.8794	5.9490	5.9126	5.9519
9.09	5.8415	6.0807	5.6626	5.6868
8.26	5.7341	5.9204	5.6812	5.6892

This figure "figure1.jpg" is available in "jpg" format from:

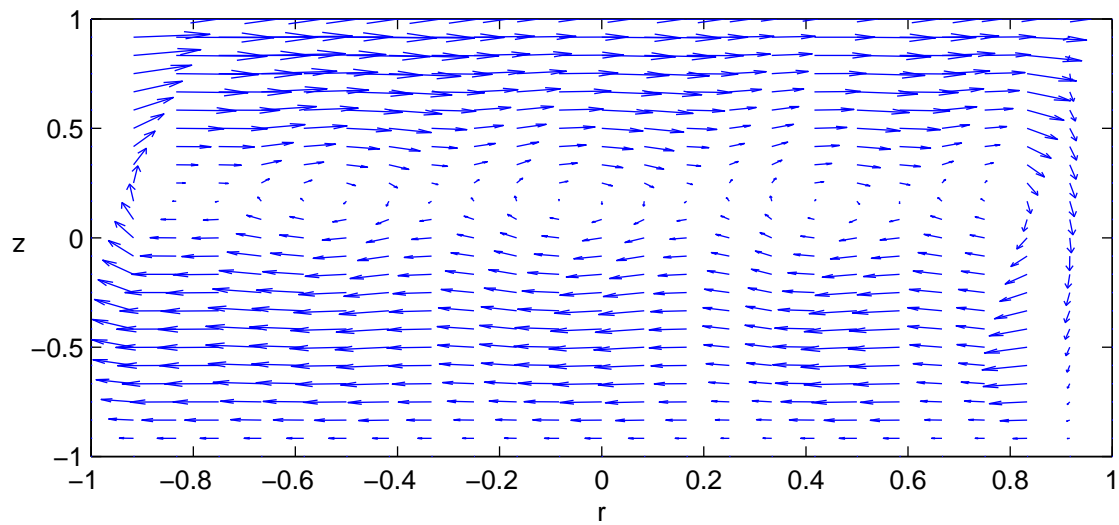
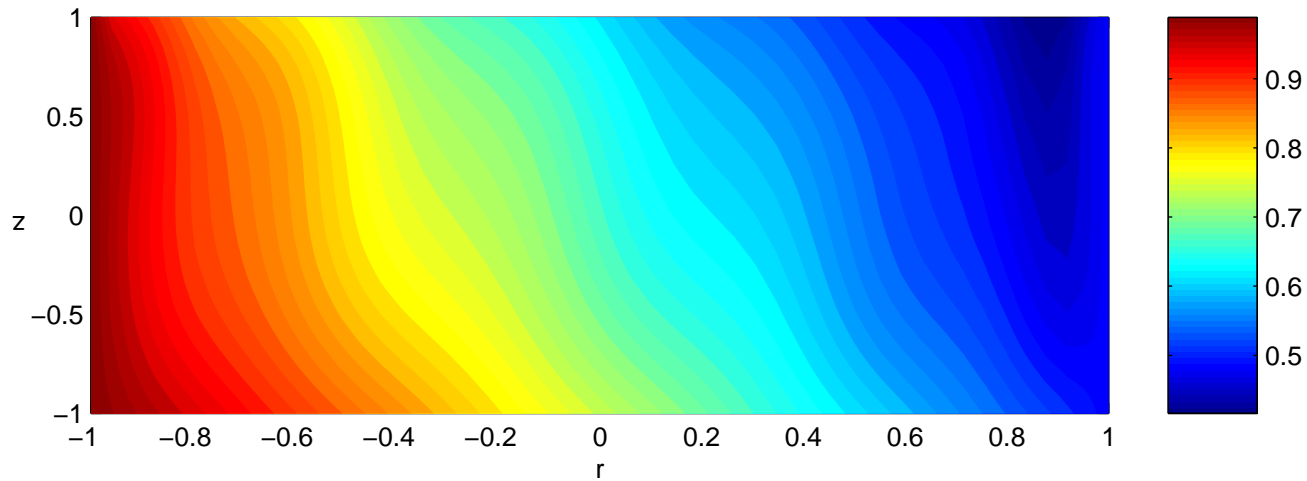
<http://arxiv.org/ps/math/0110195v2>

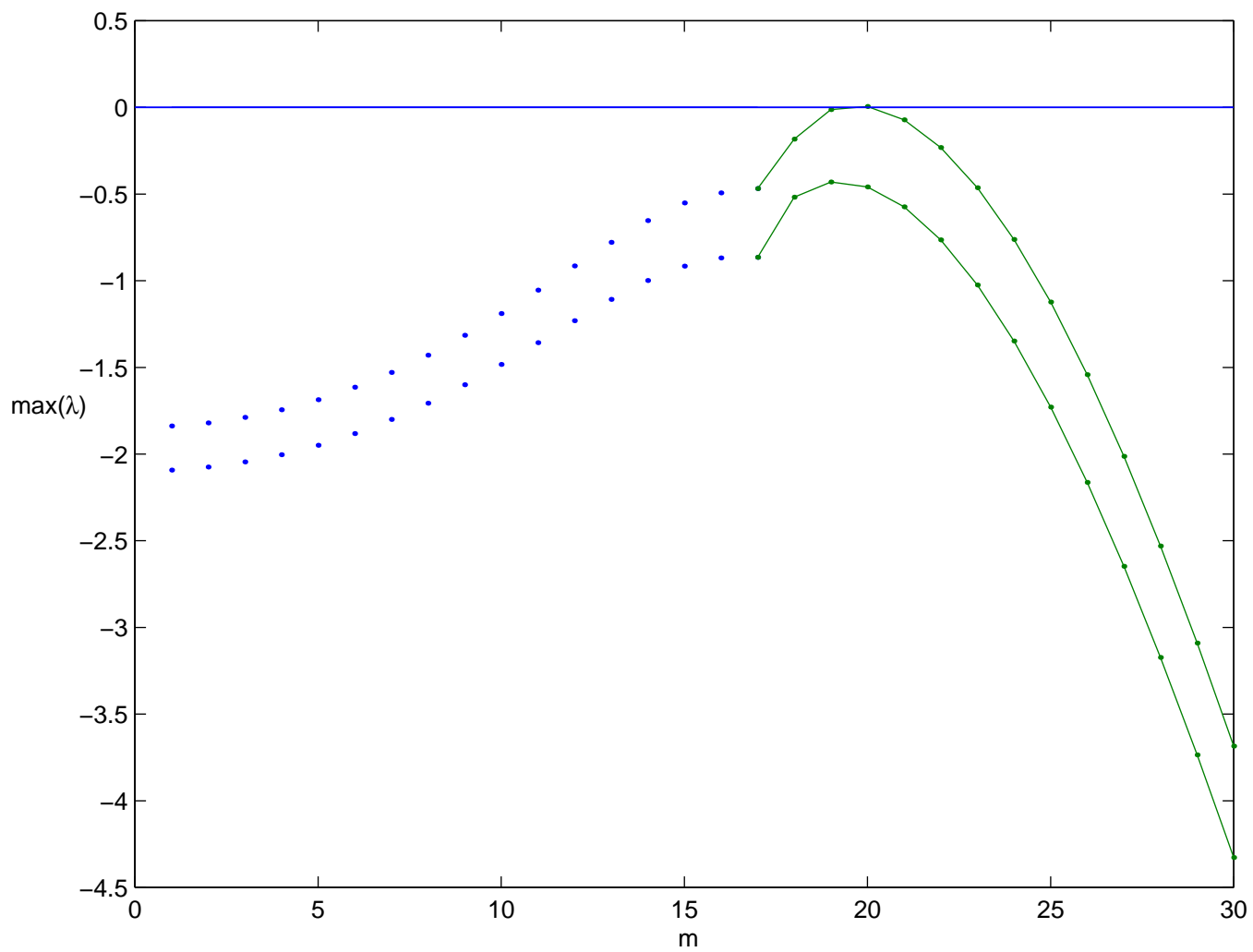




This figure "figure4.gif" is available in "gif" format from:

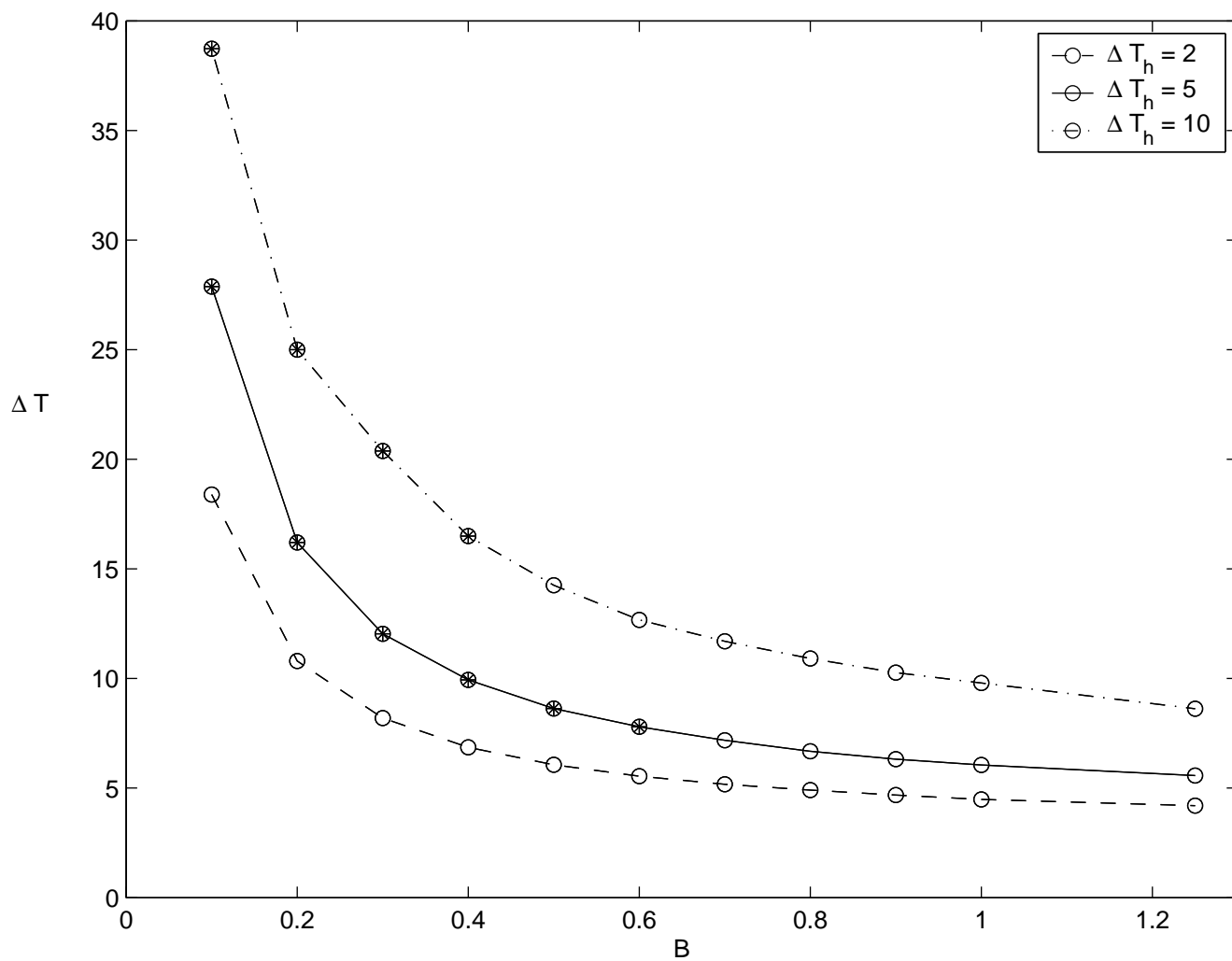
<http://arxiv.org/ps/math/0110195v2>

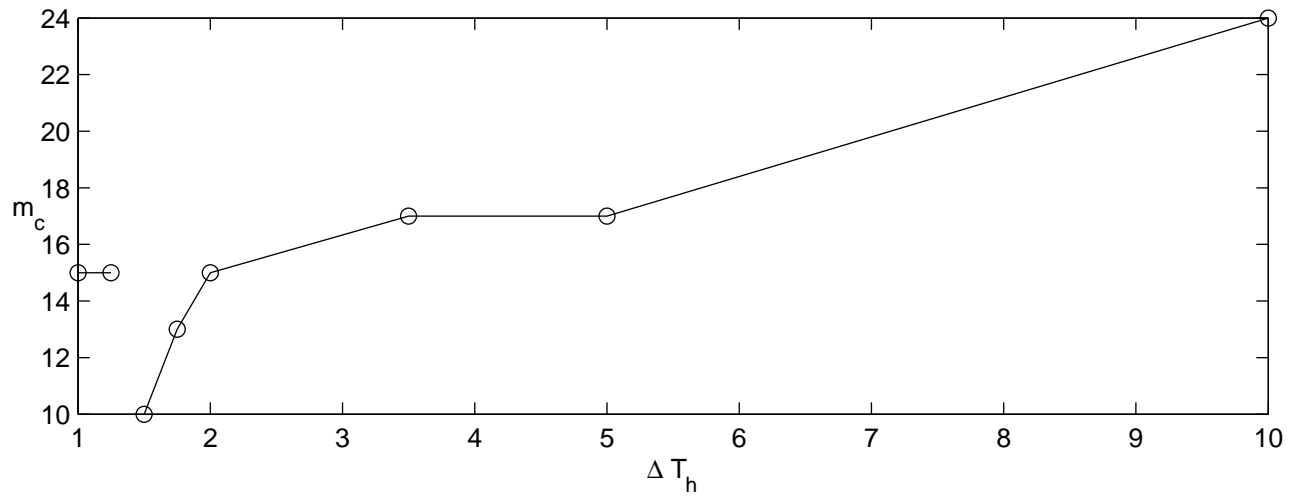
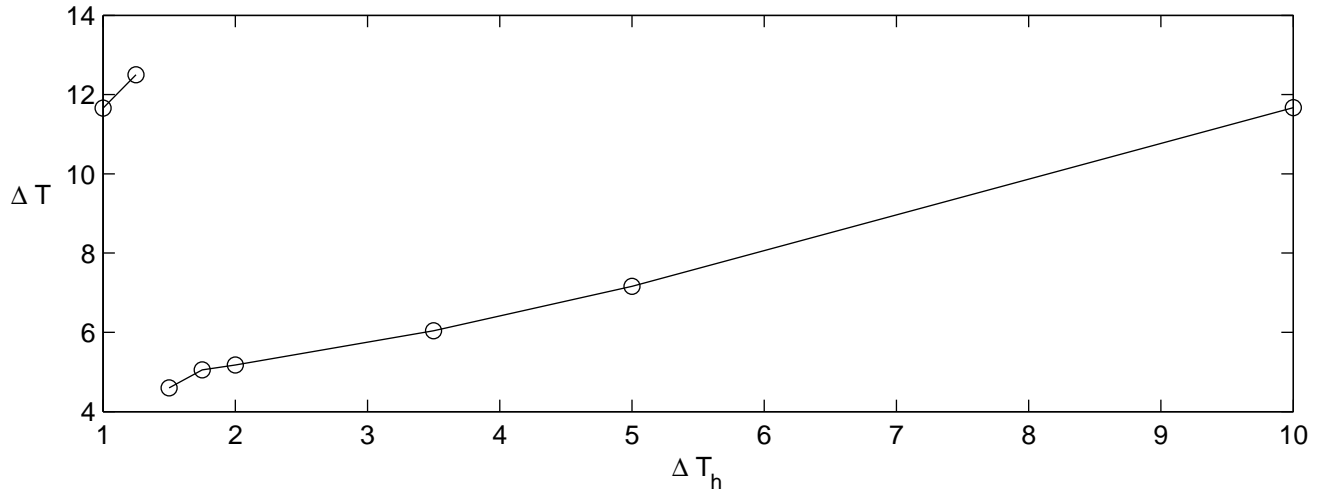




This figure "figure7.jpg" is available in "jpg" format from:

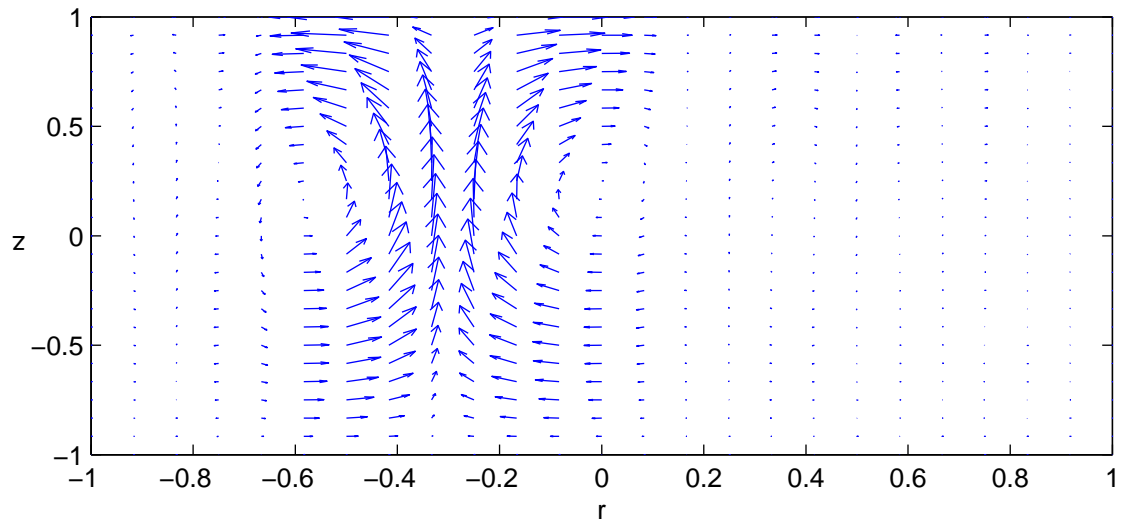
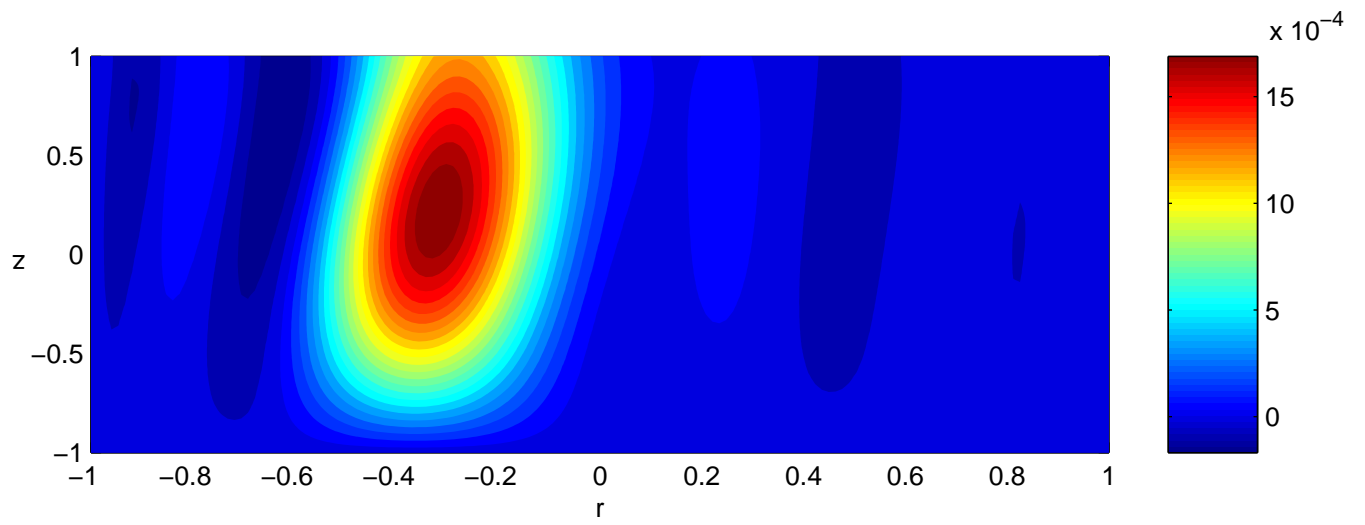
<http://arxiv.org/ps/math/0110195v2>





This figure "figure10.jpg" is available in "jpg" format from:

<http://arxiv.org/ps/math/0110195v2>



This figure "figure12.jpg" is available in "jpg" format from:

<http://arxiv.org/ps/math/0110195v2>

This figure "figure13.jpg" is available in "jpg" format from:

<http://arxiv.org/ps/math/0110195v2>